International Journal of Minerals, Metallurgy and Materials
Volume 27, Number 7, July 2020, Page 996
https://doi.org/10.1007/s12613-019-1962-y

Metal-doped $(Cu,Zn)Fe_2O_4$ from integral utilization of toxic Zn-containing electric arc furnace dust: An environment-friendly heterogeneous Fenton-like catalyst

Jun-wu Li[1)], *Xing Han*[1)], *Rong-xia Chai*[1)], *Fang-qin Cheng*[2)], *Mei Zhang*[1)], *and Min Guo*[1)]

1) State Key Laboratory of Advanced Metallurgy, School of Metallurgical and Ecological Engineering, University of Science and Technology Beijing, Beijing 100083, China

2) Shanxi Collaborative Innovation Center of High Value-added Utilization of Coal-related Wastes, Shanxi University, Shanxi 030006, China

(Received: 8 October 2019; revised: 14 November 2019; accepted: 15 November 2019)

Abstract: Pure metal-doped $(Cu,Zn)Fe_2O_4$ was synthesized from Zn-containing electric arc furnace dust (EAFD) by solid-state reaction using copper salt as additive. The effects of pretreated EAFD-to-$Cu_2(OH)_2CO_3{\cdot}6H_2O$ mass ratio, calcination time, and calcination temperature on the structure and catalytic ability were systematically studied. Under the optimum conditions, the decolorization efficiency and total organic carbon (TOC) removal efficiency of the as-prepared ferrite for treating a Rhodamine B solution were approximately 90.0% and 45.0%, respectively, and the decolorization efficiency remained 83.0% after five recycles, suggesting that the as-prepared $(Cu,Zn)Fe_2O_4$ was an efficient heterogeneous Fenton-like catalyst with high stability. The high catalytic activity mainly depended on the synergistic effect of iron and copper ions occupying octahedral positions. More importantly, the toxicity characteristic leaching procedure (TCLP) analysis illustrated that the toxic Zn-containing EAFD was transformed into harmless $(Cu,Zn)Fe_2O_4$ and that the concentrations of toxic ions in the degraded solution were all lower than the national emission standard (GB/31574—2015), further confirming that the as obtained sample is an environment-friendly heterogeneous Fenton-like catalyst.

Keywords: Zn-containing electric arc furnace dust; metal-doped Cu−Zn ferrite; heterogeneous Fenton-like catalyst; environmental effect

1. Introduction

Zn-containing electric arc furnace dust (EAFD) is a toxic solid waste produced in the process of electric steelmaking [1−3]. Because the dust is mainly composed of Fe, Zn, and some trace heavy metal elements such as Pb, Cr, and Cd, traditional treatment methods have mainly included solidification, pyrometallurgical, and hydrometallurgical processes. In the solidification approach, EAFD is mixed with clay or cement evenly and cured at a certain temperature before landfill treatment; although the process flow is simple, this method cannot extract valuable metals from the Zn-containing EAFD, which may damage soil through re-leaching of toxic substances over time [4]. In pyrometallurgical and hydrometallurgical processes, Zn resources are extracted by reducing $ZnFe_2O_4$ at high temperatures [5] and acid/alkali leaching of Zn into solution [6], respectively. Unfortunately, these methods suffer drawbacks of high energy consumption for the pyrometallurgical process and a lengthy procedure and poor selectivity for the hydrometallurgical process; these shortcomings have restricted the development of these approaches [7]. Balancing the advantages of these methods is a current goal of researchers in this field. However, the use of green processes for overall utilization of Zn-containing EAFD has rarely been reported.

Spinel ferrite is an important inorganic functional material with the advantages of good thermal stability, good dielectric property, high resistivity, and high corrosion resistance. It is widely used in various fields applications [8]. In our previous study [9−10], spinel ferrite $(Ni,Zn)Fe_2O_4$ was synthesized from Zn-containing EAFD by a solid-state reaction method; the product exhibited good magnetic properties, with a high saturation magnetization of 60.5 $emu{\cdot}g^{-1}$ and low coercivity of 49.8 Oe. Unfortunately, no work has been done on the preparation of ferrite-based heterogeneous Fenton-like catalysts from EAFD.

Traditional Fenton oxidation is an advanced oxidation technology that combines Fe^{2+} and H_2O_2 to produce •OH rad-

Corresponding author: Min Guo E-mail: guomin@ustb.edu.cn

icals for degrading organic wastewater, as depicted in Eqs. (1)–(3):

$$Fe^{2+}/\equiv Fe^{2+} + H_2O_2 \rightarrow Fe^{3+}/\equiv Fe^{3+} + \bullet OH + OH^- \quad (1)$$

$$Fe^{3+}/\equiv Fe^{3+} + H_2O_2 \rightarrow Fe^{2+}/\equiv Fe^{2+} + HO_2\bullet + H^+ \quad (2)$$

$$\bullet OH + RhB \rightarrow \text{degraded products} \quad (3)$$

It has the advantages of convenient operation, a high oxidation rate, and no selectivity toward the oxidized substance; however, this process also has several disadvantages, such as strong acidic conditions, difficulty recycling Fe^{2+}, and the formation of large amounts of iron sludge during the reaction, which greatly increases the cost of wastewater treatment. To overcome these shortcomings, researchers have developed heterogeneous Fenton oxidation technology using an easily separable solid catalyst instead of Fe^{2+} ions, and some ferrites with suitable magnetic properties and high stability have been investigated as efficient heterogeneous Fenton catalysts [11–14]. Unfortunately, compared with the reaction rate between Fe^{2+} and H_2O_2 with a homogeneous Fenton catalyst that between Fe^{2+} in the ferrite and H_2O_2 is slower (Eq. (2)), which results in longer degradation time for organic dyes. Under this circumstance, external fields such as light, electricity, and microwaves have been used in conjunction with the ferrite to increase its catalytic rate [15]. Sharma and Singhal [16] synthesized a $CuFe_2O_4$ catalyst from pure $Fe(NO_3)_3{\cdot}9H_2O$ and $Cu(NO_3)_3{\cdot}3H_2O$ via a sol–gel method, the degradation efficiency of the ferrite for treating 2-NP were higher (80% in 30 min under visible light) than that in the absence of light (54% in 30 min) in a reaction system of dye + H_2O_2. More importantly, doping metallic ions into ferrites can improve their catalytic performance [17]. Given that the standard electrode potential of Cu^{2+}/Cu^+ (0.15 V vs. standard hydrogen electrode (SHE)) is lower than that of Fe^{3+}/Fe^{2+} (0.77 V vs. SHE) at 298 K, doping Cu^{2+} into pure $ZnFe_2O_4$ can promote the circulation of Fe^{3+}/Fe^{2+} and improve its catalytic efficiency (Eqs. (4)–(5)).

$$\equiv Cu^{2+} + HO_2\bullet \rightarrow \equiv Cu^+ + H^+ + O_2 \quad (4)$$

$$\equiv Cu^+ + \equiv Fe^{3+} \rightarrow \equiv Cu^{2+} + \equiv Fe^{2+} \quad (5)$$

Huang *et al.* [18] prepared the ferrite $(Cu_{0.8}Zn_{0.2})Fe_2O_4$ using pure $Fe(NO_3)_3{\cdot}9H_2O$, $Cu(NO_3)_2{\cdot}2.5H_2O$, and $Zn(NO_3)_2{\cdot}6H_2O$ and found that the product could degrade more than 95% of atrazine in 30 min. Zhao *et al.* [19] found that doping Cu into pure $ZnFe_2O_4$ substantially enhances its photocatalytic performance. Under optimal conditions, the degradation efficiency for treating Orange II was approximately 90% in 30 min. Because the main phases of Zn-containing EAFD are spinel-structured $ZnFe_2O_4$ and Fe_3O_4, transforming the Zn-containing EAFD into pure $(Zn,Cu)Fe_2O_4$ is feasible, which would not only decrease the preparation cost but also enable the full utilization of the dust.

In this paper, metal-doped $(Cu,Zn)Fe_2O_4$ spinel ferrite was successfully synthesized from pretreated Zn-containing EAFD and $Cu_2(OH)_2CO_3{\cdot}6H_2O$ as an additive using a solid-state reaction approach. The influences of the experimental conditions on the preparation of $(Cu,Zn)Fe_2O_4$ and on its catalytic properties were studied in detail. Moreover, the catalytic mechanism of as-prepared ferrite was also discussed. This paper may provide a green and cost-effective way to integrally utilize the metallurgical solid wastes for high performance heterogeneous Fenton catalyst.

2. Experimental

2.1. Raw materials

The Zn-containing EAFD used in experiments was supplied by the Tianjin Pipe (Group) Corporation, China. The element components of EAFD were mainly Fe, Zn, Ca, Si, and trace quantities of Pb and Cr, as shown in Table 1; the major crystalline phases were $ZnFe_2O_4$, Fe_3O_4, $CaCO_3$, KCl, and SiO_2, as shown in curve (a) in Fig. 1. The dusts comprised spherical particles that had agglomerated to some extent (Fig. 2(a)). In addition, analytical-grade reagents including HCl (36wt%–38wt%), H_2O_2 (30wt%), Rhodamine B (RhB), and ethanol were purchased from Sinopharm of China and were used without further purification.

Table 1. Chemical compositions of Zn-containing EAFD and pretreated EAFD by XRF analysis wt%

Material	Fe	Zn	Ca	Si	K	Cl	Pb	Cr
Zn-containing EAFD	37.29	7.79	5.33	2.21	3.11	2.63	1.16	0.16
Pretreated EAFD	50.03	8.59	0.31	2.91	0.15	0.09	1.21	0.20

2.2. Experimental procedure

2.2.1. Pretreatment of Zn-containing EAFD

First, 20 g of Zn-containing EAFD was mixed with 200 mL of 0.5 mol·L^{-1} HCl solution in a beaker and the resulting mixture was transferred to an electromagnetic stirrer and stirred at 900 r/min for 15 h at room temperature. Second, the solid and liquid were separated by centrifugation (TGL-16, China) at 5000 r/min for 10 min. Third, the obtained solid was dried in a drying oven at 100°C for 10 h. Curve (b) in Fig. 1 indicates that the major phases of the pretreated EAFD were $ZnFe_2O_4$, Fe_3O_4, and SiO_2; $CaCO_3$ and KCl in the EAFD were washed away after treatment. The morphology of pretreated EAFD remained nearly unchanged compared with that of the Zn-containing EAFD (Fig. 2(b)).

2.2.2. Synthesis of Cu–Zn ferrite

To synthesize pure ferrite, the molar ratio between the +2

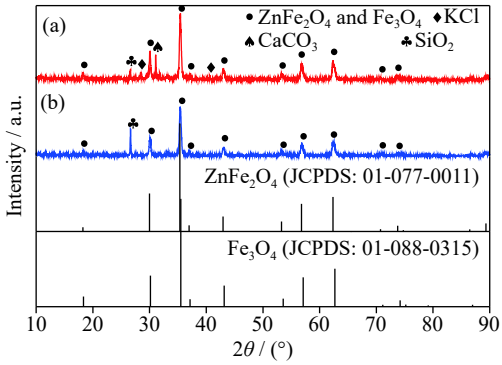

Fig. 1. XRD patterns of (a) Zn-containing EAFD and (b) pretreated EAFD.

ions and the +3 ions should be controlled at 1:2 on the basis of the chemical formula of the ferrite (MFe_2O_4). The molar ratio in the pretreated EAFD was less than 1:2 (Table 1); thus, a salt containing M^{2+} ions needed to be added to the dust. $Cu_2(OH)_2CO_3{\cdot}6H_2O$ was chosen as the additive because Cu^{2+} has catalytic effects and because it can be decomposed to CuO and CO_2 while not producing toxic substances at high temperatures during the preparation process. In detail, 2.0 g of pretreated EAFD was first mixed with 0.8, 0.9, or 1.0 g $Cu_2(OH)_2CO_3{\cdot}6H_2O$ in an alumina crucible. After the components were evenly mixed, the crucible was transferred to a muffle furnace at room temperature (25°C). The furnace was then heated to 1000°C gradually, maintained at this temperature for 2 h, then cooled to room temperature. Finally, the reaction products were ground into powders for further experiments. The overall flow chart for the synthesis of the Cu−Zn ferrite is illustrated in Fig. 3.

2.2.3. Catalytic reaction

In the catalytic degradation experiments, 200 mL of RhB solution diluted to a concentration of 10 mg·L^{-1} (C_0) was added to a 250 mL beaker and the initial absorbance of the RhB (A_0) was measured. A certain amount of the synthetic sample was then added to the RhB solution and stirred continuously with an agitator (NP20L, China) at 200 r/min for 30 min under dark conditions. A certain amount of H_2O_2 was subsequently added to the solution by pipette, and the suspension was immediately irradiated with visible light with an intensity of 20 W. Every 30 min, 5.0 mL of the solution was collected from the reaction system into a centrifuge tube and centrifuged at 3000 r/min for 5 min for solid–liquid separation. The absorbance of the RhB solution at 554 nm (A_t) was measured using a spectrophotometer (722S, China). The decolorization efficiency (η) of the RhB and the reaction rate constant k (min^{-1}) were obtained from Eqs. (6) and (7), respectively:

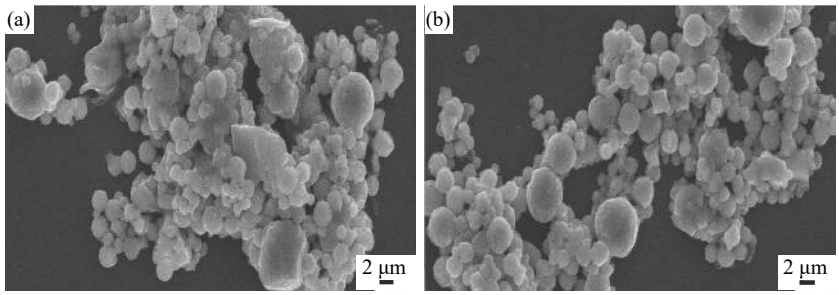

Fig. 2. SEM images of (a) Zn-containing EAFD and (b) pretreated EAFD.

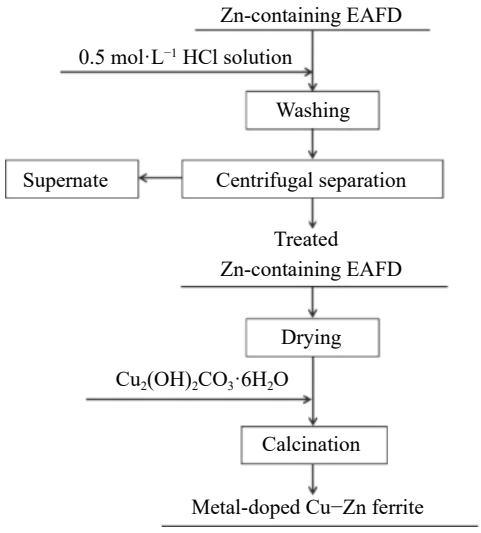

Fig. 3. Overall flow chart for the synthesis of Cu−Zn ferrite.

$$\eta = (A_0 - A_t)/A_0 \times 100\% \quad (6)$$

$$k \cdot t = \ln(C_0/C_t) \quad (7)$$

All of the catalytic reaction temperatures were controlled at 25°C with a water bath (HH-6, China).

2.3. Characterization

The mineralogical phases and elements of the Zn-containing EAFD and the pretreated EAFD were determined by X-ray diffraction (XRD, Rigaku Dmax 2500 PC, Japan) and X-ray fluorescence (XRF, XRF-1800, Japan), respectively. The crystalline structures of the as-synthesized samples and the samples after five cycles of catalytic degradation experiments were characterized by XRD. The micromorphology of the EAFD, treated EAFD, and as-synthesized samples were characterized by scanning electron microscopy (SEM, SUPRA 55, Germany).

3. Results and discussion

3.1. Effect of preparation parameters on the synthesis of metal-doped Cu−Zn ferrite and catalytic capability

3.1.1. Effect of the pretreated EAFD to $Cu_2(OH)_2CO_3{\cdot}6H_2O$ mass ratio

Fig. 4 shows the crystalline properties and composition of synthetic catalysts with different pretreated EAFD-to-$Cu_2(OH)_2CO_3{\cdot}6H_2O$ mass ratios ($R_{EAFD/Cu}$). When the $R_{EAFD/Cu}$ was controlled at 2.0:0.8 or 2.0:0.9, peaks appeared at 2θ values of 79.0°, 74.0°, 71.0°, 62.5°, 57.0°, 53.4°, 43.1°, 37.0°, 35.4°, 30.1°, and 18.3°; these peaks were indexed to the (444), (533), (620), (440), (511), (422), (400), (222), (311), (220), and (111) crystallographic planes of $(Cu_{0.5}Zn_{0.5})Fe_2O_4$ (JCPDS: 01-077-0012), respectively. No other phases were detected, confirming that pure (Zn,Cu)Fe_2O_4 with good crystallinity was obtained according to Eq. (8):

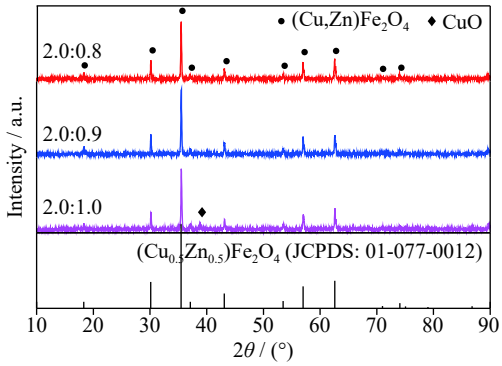

Fig. 4. XRD patterns of synthetic samples with varying $R_{EAFD/Cu}$ values.

$$\frac{x}{2}Cu_2(OH)_2CO_3\cdot 6H_2O + \frac{2x}{3}Fe_3O_4 + yZnFe_2O_4 + \frac{x}{6}O_2 \rightarrow (Cu_xZn_y)Fe_2O_4 + \frac{x}{2}CO_2 + \frac{7x}{2}H_2O \quad (8)$$

When the $R_{EAFD/Cu}$ was increased to 2.0:1.0, the diffraction peaks of CuO appeared. The appearance of CuO was mainly attributed to the decomposition of excessive $Cu_2(OH)_2CO_3{\cdot}6H_2O$ into CuO at the high calcination temperature (1000°C), as depicted in Eq. (9):

$$Cu_2(OH)_2CO_3{\cdot}6H_2O \rightarrow 2CuO + CO_2 + 7H_2O \quad (9)$$

Moreover, the obtained samples exhibited an irregular morphology and different sizes, some of which were agglomerated under different $R_{EAFD/Cu}$ values, as illustrated in Figs. 5(a)–5(c).

The influences of $R_{EAFD/Cu}$ on the catalytic properties of the synthetic catalysts are given in Fig. 6, and the degradation system for treating 10 mg·L^{-1} RhB solution was 0.2 g sample + 2.0 mL H_2O_2 + 200 mL + 10 mg·L^{-1} RhB solution assisted by visible light irradiation. When the $R_{EAFD/Cu}$ was changed from 2.0:0.8 to 2.0:0.9, the decolorization efficiency increased from 61.0% to 90.0%, suggesting that the Cu−Zn ferrite obtained with $R_{EAFD/Cu}$ of 2.0:0.9 was an efficient heterogeneous catalyst for treating the RhB solution. However, when the $R_{EAFD/Cu}$ was further changed to 2.0:1.0, the degradation efficiency decreased from 90.0% to 77.0%, possibly because of the formation of a mixture of (Zn,Cu)Fe_2O_4 and CuO. The CuO produced by excessive $Cu_2(OH)_2CO_3{\cdot}6H_2O$ at high temperatures might have coated the ferrite surface and reduced the accessibility of the active reaction sites in the ferrite, resulting in poor catalytic ability. Thus, we chose $R_{EAFD/Cu}$ = 2.0:0.9 for the next experiments.

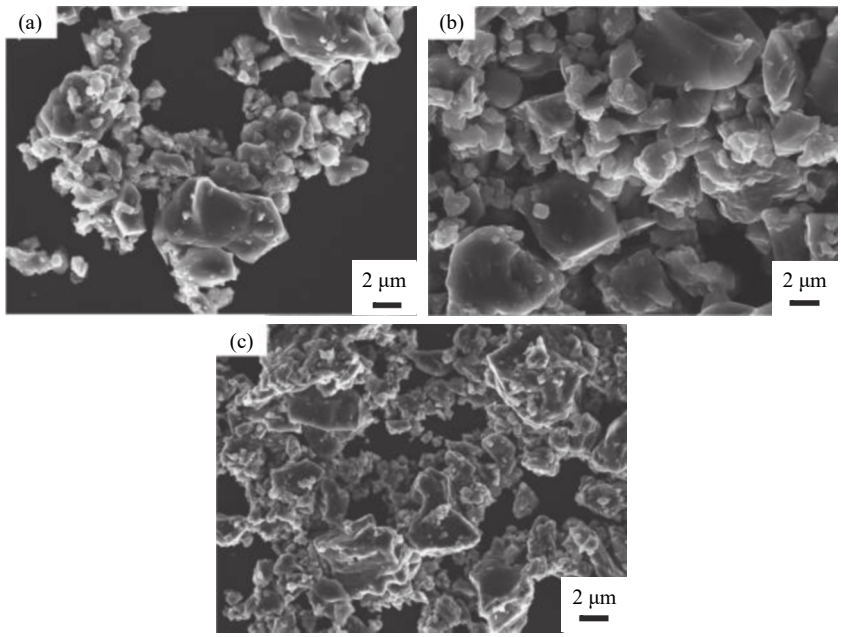

Fig. 5. SEM images of the samples prepared using various $R_{EAFD/Cu}$ values: (a) 2.0:0.8; (b) 2.0:0.9; (c) 2.0:1.0.

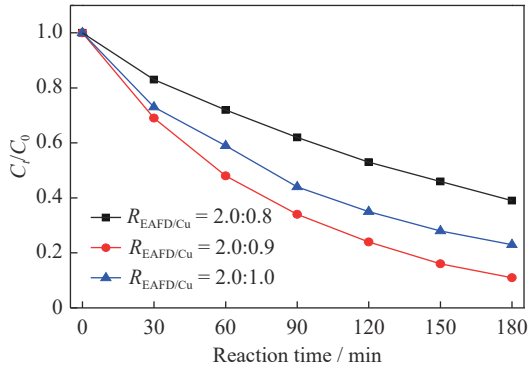

Fig. 6. Effect of different $R_{EAFD/Cu}$ values on the decolorization efficiency of an RhB solution (25°C, catalyst concentration of 1.00 g·L^{-1}, H_2O_2 dosage of 1.00vol%, and pH 6.78).

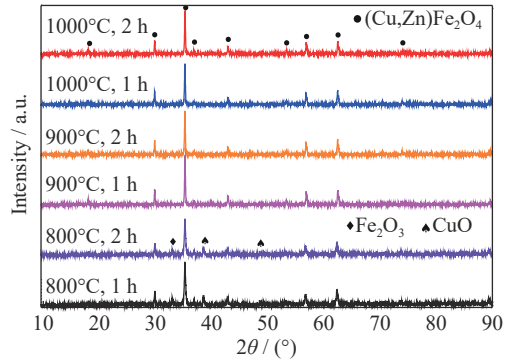

Fig. 7. XRD patterns of the catalysts prepared under different conditions.

3.1.2. Effects of calcination temperature and time

To explore how different calcination temperatures and time periods influenced the crystal phases of ferrites and the decolorization efficiencies of RhB solution, further experiments were conducted at $R_{EAFD/Cu}$ = 2.0:0.9 and the calcination temperature and time were controlled at 1000, 900, and 800°C for 2 and 1 h. The XRD patterns of the prepared samples are shown in Fig. 7. When the conditions were 1000°C for 2 or 1 h or 900°C for 2 or 1 h, all of the diffraction peaks of the samples were consistent with $(Cu_{0.5}Zn_{0.5})Fe_2O_4$ (JCPDS: 01-077-0012) and no other peaks were detected, indicating that all the obtained samples were pure ferrites. The chemical compositions of the ferrite catalysts formed under conditions of 1000°C for 2 or 1 h or 900°C for 2 or 1 h are summarized in Table 2. The chemical formulas of these samples were all approximately $Cu_{0.68}Zn_{0.32}Fe_2O_4$, demonstrating that the calcination temperature and time (1000°C for 2 or 1 h or 900°C for 2 or 1 h) did not affect the chemical compositions of the prepared ferrites.

Table 2. Chemical compositions of synthetic catalysts under different conditions ($R_{EAFD/Cu}$ = 2.0:0.9), as determined by XRF analysis mol%

Condition	Fe	Zn	Cu	Si	K	Ca	Pb	Cr
1000°C, 2 h	65.4	10.6	22.1	0.05	8.3×10^{-3}	8.8×10^{-4}	4.7×10^{-3}	2.6×10^{-3}
900°C, 2 h	65.4	10.6	22.1	0.05	8.2×10^{-3}	7.9×10^{-4}	5.7×10^{-3}	3.3×10^{-3}
1000°C, 1 h	65.4	10.6	22.1	0.05	9.1×10^{-3}	7.7×10^{-4}	5.5×10^{-3}	2.8×10^{-3}
900°C, 1 h	65.4	10.6	22.1	0.05	8.7×10^{-3}	8.1×10^{-4}	6.1×10^{-3}	4.1×10^{-3}

We doped Ca, Si, Pb, and Cr (Table 2) into the spinel-structured Cu−Zn ferrite. When the calcination temperature decreased to 800°C, other diffraction peaks assigned to Fe_2O_3 and CuO appeared in addition to those of the Cu−Zn ferrite, suggesting that the samples prepared at 800°C for 2 or 1 h were not pure ferrite. Moreover, the SEM images (Fig. 8) show that the particle sizes of the ferrites decreased dramatically and that the size distribution became narrower when the reaction temperature was changed from 1000 to 900°C, which should enhance the catalytic performance of the obtained ferrites in theoretical.

Fig. 9 presents the catalytic properties of the samples prepared under different temperatures and time periods. In the reaction systems of 0.2 g ferrite + 2 mL H_2O_2 + 200 mL 10 mg·L^{-1} RhB solution assisted by visible light irradiation, the ferrite prepared at 1000°C for 2 h, which exhibited a relatively large size (Fig. 8(a)), exhibited the best decolorization efficiency of 90.0% for treating RhB solution compared with the other three samples. This phenomenon is inconsistent with the consensus that a catalyst with higher specific surface area generally exhibits higher catalytic performance. Elucidation of the catalytic reaction mechanism of the synthetic $(Cu,Zn)Fe_2O_4$ in the system of catalyst + H_2O_2 + visible light + RhB solution is necessary to explain this experimental result.

3.2. Catalytic reaction mechanism of as-synthesized Cu−Zn ferrite catalyst in reaction system of catalyst + H_2O_2 + visible light + RhB solution

In general, the main factors that determine the catalytic performance of ferrite include chemical composition, specific surface area, and ion occupation. According to Table 2, the chemical formulas of the samples under different temperatures and time periods were approximately $Cu_{0.68}Zn_{0.32}Fe_2O_4$, which demonstrates that the calcination temperature and time did not affect the chemical compositions of the prepared ferrites. In addition, the catalyst calcined at 900°C for 1 h exhibited the smallest particle size among the four prepared catalysts (Fig. 8); thus, the catalyst calcined at 900°C for 1 h should theoretically demonstrate greater removal efficiency of RhB because it has more active sites exposed; however, a different result was obtained. Therefore, on the basis of the

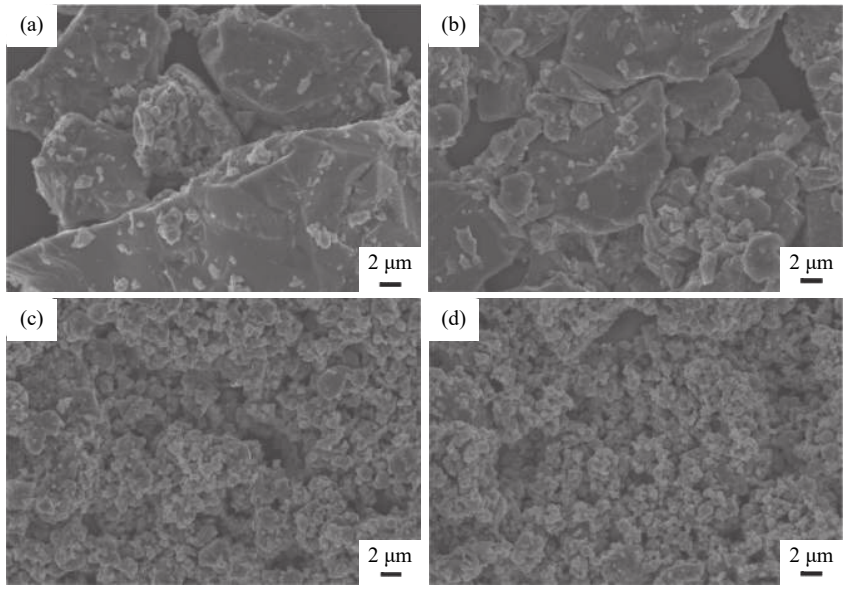

Fig. 8. SEM images of the samples prepared under different conditions: (a) 1000°C, 2 h; (b) 1000°C, 1 h; (c) 900°C, 2 h; (d) 900°C, 1 h.

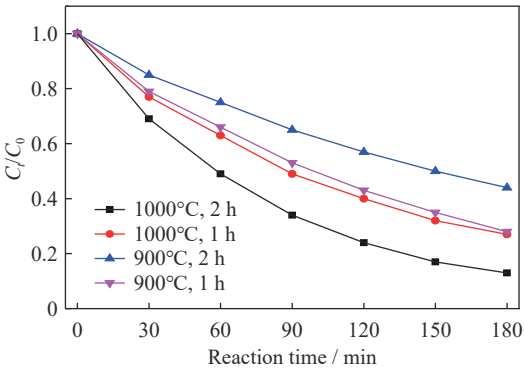

Fig. 9. Effects of calcination temperature and time on the decolorization efficiency of RhB solution (25°C, catalyst concentration of 1.00 g·L^{-1}, H_2O_2 dosage of 1.00vol%, and pH 6.78).

aforementioned analysis, the amounts of metallic ions occupying octahedral (Oct) positions and tetrahedral (Tet) positions in the ferrite catalyst might play an important part in determining the catalytic performance.

To semi-quantitatively characterize the occupation of metallic ions, the ferrites were analyzed by XPS; the results are presented in Fig. 10. The survey XPS spectrum of the (Cu,Zn)Fe_2O_4 ferrites confirmed the coexistence of Cu, Zn, Fe, and O (Fig. 10(a)). In the high-resolution spectra of Fe 2p (Fig. 10(b)), the peaks at 710.5 eV, which are attributed to Fe $2p_{3/2}$, can be deconvoluted into two peaks at approximately 710.3 and 712.7 eV, corresponding to Fe^{3+}_{Oct} and Fe^{3+}_{Tet} [20–21]. In the Cu 2p spectral region (Fig. 10(c)), the binding-energy peaks ascribed to Cu $2p_{3/2}$ at 933.7 eV were also deconvoluted into two components corresponding to the Cu $2p_{3/2}$ of Cu^{2+}_{Oct} and Cu^{2+}_{Tet} [22–23]. As shown in Fig. 10(d), the characteristic peaks of Zn $2p_{3/2}$ at 1021.2 eV can be divided into two peaks at approximately 1021.0 and 1021.8 eV, corresponding to Zn^{2+}_{Tet} and Zn^{2+}_{Oct}, respectively [24]. Because the catalytic performance of the prepared ferrites mainly depended on the amount of Fe^{3+}_{Oct} and Cu^{2+}_{Oct}, the occupation ratio of Fe^{3+}_{Oct} and Cu^{2+}_{Oct}, as well as the sum of Fe^{3+}_{Oct} and Cu^{2+}_{Oct}, is included in Table 3. The results show that the decolorization efficiency increases with increasing sum of Fe^{3+}_{Oct} and Cu^{2+}_{Oct}. The catalyst calcined at 900°C for 2 h exhibited the lowest Fe^{3+}_{Oct} (42.6%) and the smallest sum of Fe^{3+}_{Oct} and Cu^{2+}_{Oct} (109.9%); it therefore exhibited the lowest degradation efficiency of 56.0%. By contrast, both the catalyst calcined at 1000°C for 1 h and that calcined at 900°C for 1 h had approximately the sum of Fe^{3+}_{Oct} and Cu^{2+}_{Oct}; thus, their decolorization efficiencies were about the same(73.8%, 72.5%). Notably, although the catalyst calcined at 1000°C for 2 h did not have the maximum Fe^{3+}_{Oct}, it had the maximum sum of Fe^{3+}_{Oct} and Cu^{2+}_{Oct} (130.6%); it therefore exhibited the highest decolorization efficiency (90.0%). This result may be due to a synergistic effect of Fe^{3+}_{Oct} and Cu^{2+}_{Oct} according to Eqs. (4)–(5). Under this circumstance, more •OH species were generated; the ferrite $(Cu_{0.68}Zn_{0.32})Fe_2O_4$ prepared at 1000°C for 2 h therefore exhibited the best catalytic efficiency.

3.3. Effect of catalytic conditions on the decolorization of RhB

3.3.1. Catalyst concentration

The influence of catalyst concentration on the decolorization efficiency of RhB is shown in Fig. 11. As the catalyst concentration was varied from 0.50 to 1.00 g·L^{-1}, the decolorization efficiency of RhB and the k_{app} (chemical reaction rate constant) increased from 69.0% to 90.0% and from 0.0063 to 0.0122 min^{-1}, possibly because additional active

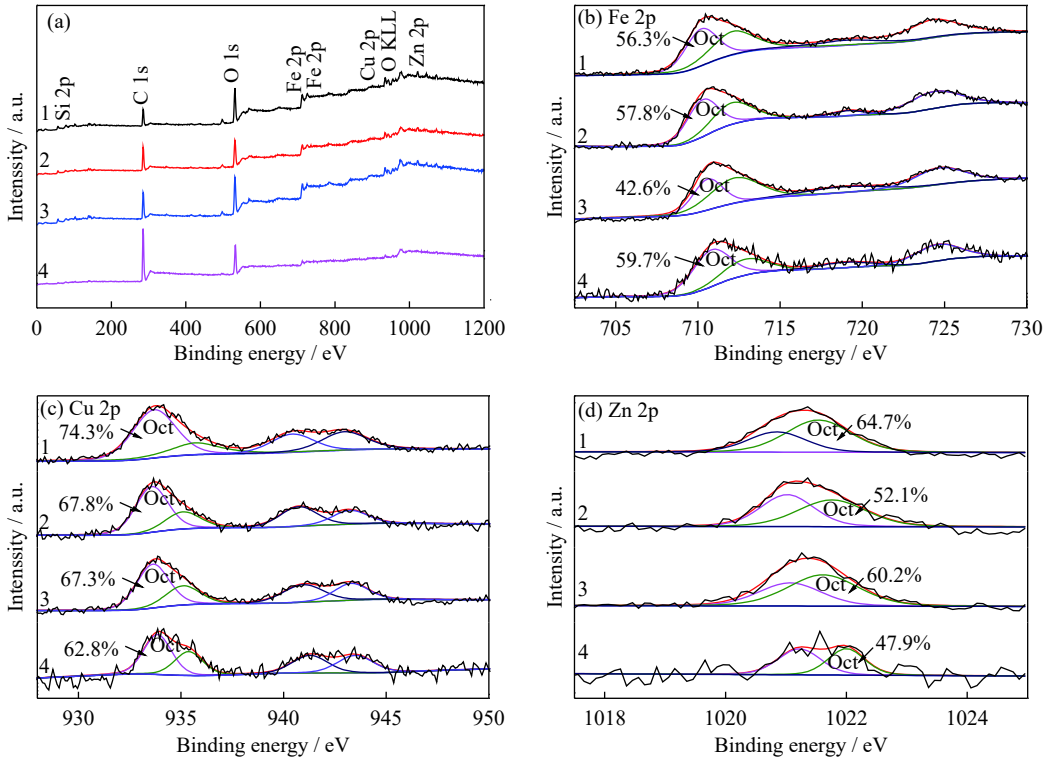

Fig. 10. XPS spectra of synthetic catalysts: (a) survey pattern of the samples; high-resolution spectra of (b) Fe 2p; (c) Cu 2p; (d) Zn 2p. 1—1000°C, 2 h; 2—1000°C, 1 h; 3—900°C, 2 h; 4—900°C, 1 h.

Table 3. Ion occupation ratios of Fe^{3+}_{Oct} and Cu^{2+}_{Oct} under different conditions determined by XRF analysis and the decolorization efficiency of RhB

Condition	Ion occupation ratio / mol%			Decolorization efficiency of RhB / %
	Fe^{3+}_{Oct}	Cu^{2+}_{Oct}	Sum	
1000°C, 2 h	56.3	74.3	130.6	90.0
1000°C, 1 h	57.8	67.8	125.6	73.8
900°C, 2 h	42.6	67.3	109.9	56.0
900°C, 1 h	59.7	62.8	122.5	72.5

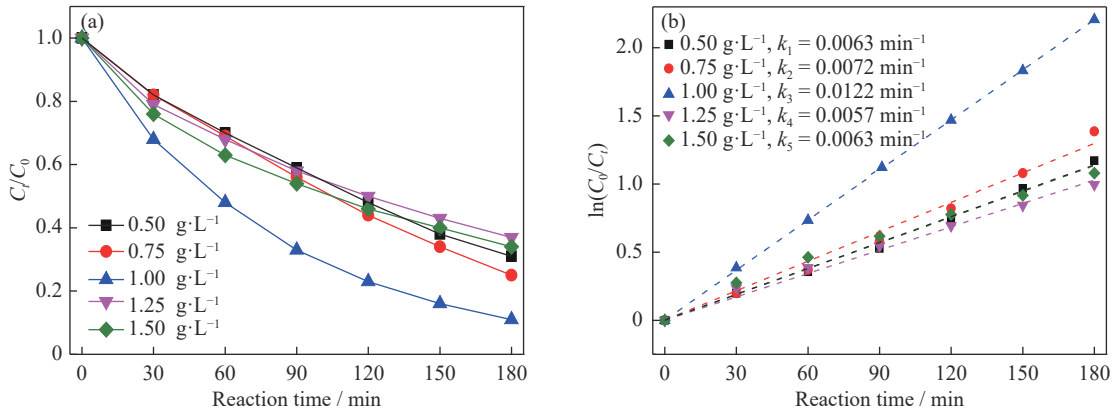

Fig. 11. Effect of catalyst concentration on (a) the decolorization efficiency of RhB and (b) the catalytic kinetics curves (25°C, H_2O_2 dosage of 1.00vol%, and pH 6.78).

sites on the ferrite surface reacted with H_2O_2 to generate more reactive radicals such as •OH, thereby leading to improved efficiency. However, when the catalyst concentration was further increased to 1.50 g·L^{-1}, the η decreased to 66.0%. This decrease may be caused by the additional active sites provided by the excess catalyst dramatically increasing the

concentration of •OH and the amount of •OH adsorbed onto the ferrite surface within a short time, increasing the probability of collision between •OH radicals (Eq. (10)) [25], finally reducing the amount of •OH and decreasing the η of RhB:

$$\bullet OH + \bullet OH \rightarrow H_2O + O_2 \quad (10)$$

3.3.2. H_2O_2 dosage

The dosage of H_2O_2 played a key role in the heterogeneous Fenton reaction. The effect of the initial H_2O_2 dosage (0.25vol%–1.50vol%) is shown in Fig. 12. When the H_2O_2 dosage ranged from 0.25vol% to 1.00vol%, more •OH radicals were generated as described in Eq. (1); thus, the η value of RhB increased from 41.0% to 90.0% and the k_{app} value increased from 0.0031 to 0.0122 min^{-1} correspondingly. However, when the H_2O_2 dosage was further increased from 1.00vol% to 1.50vol%, the removal efficiency was not improved as expected; it instead decreased from 90.0% to 77.0%, and the k_{app} decreased from 0.0122 to 0.0090 min^{-1}. This phenomenon might be due to the formed •OH radicals again reacting with added excess H_2O_2 to generate HO_2• radicals (Eq. (11)), which could also react with •OH radicals (Eq. (12)), leading to low concentration of •OH radicals [26–27]:

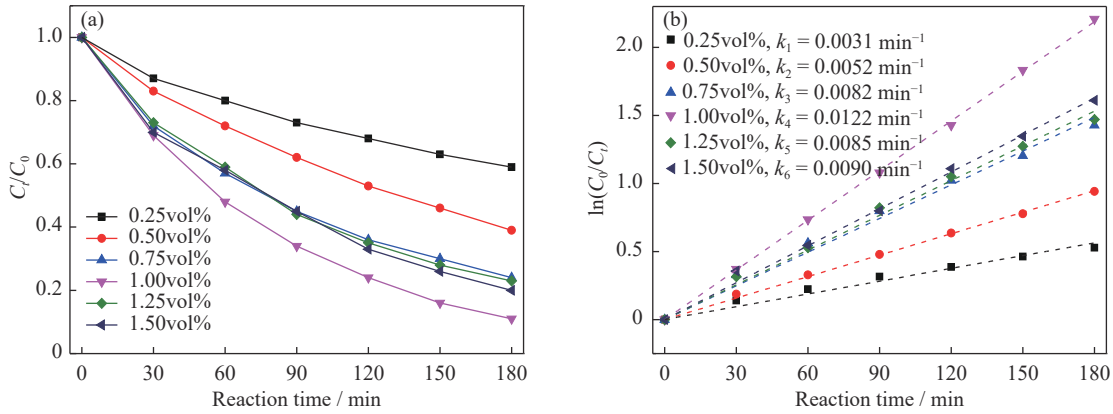

Fig. 12. Effect of H_2O_2 dosage on (a) the decolorization efficiency of RhB and (b) the catalytic kinetics curves (25°C, catalyst concentration 1.00 g·L^{-1}, and pH 6.78).

$$\bullet OH + H_2O_2 \rightarrow HO_2\bullet + H_2O \quad (11)$$

$$\bullet OH + HO_2\bullet \rightarrow H_2O + O_2 \quad (12)$$

3.3.3. Initial pH value

The initial pH value of reaction solutions is an important parameter for the decolorization of RhB. Initial pH values of 3.17, 4.35, 6.78, 8.35, and 9.62 were selected in this system, and the pH values of the solution were adjusted by addition of HCl solution or NaOH solution [28]. As observed in Fig. 13, the η reached its highest value when the initial pH value of the reaction solution was 6.78. When the pH value of the solution was varied from 6.78 to 3.17, the removal efficiency of RhB and the k_{app} decreased with decreasing pH value. In the reaction system, excessive H^+ ions could easily react with H_2O_2 to form oxonium ions by solvating a proton (Eq. (13)) [29], thereby reducing the amount of •OH radicals:

$$H^+ + H_2O_2 \rightarrow H_3O_2^+ \quad (13)$$

Moreover, increasing the initial pH value to 9.62 would lead to decomposition of the H_2O_2 in the system into H_2O and

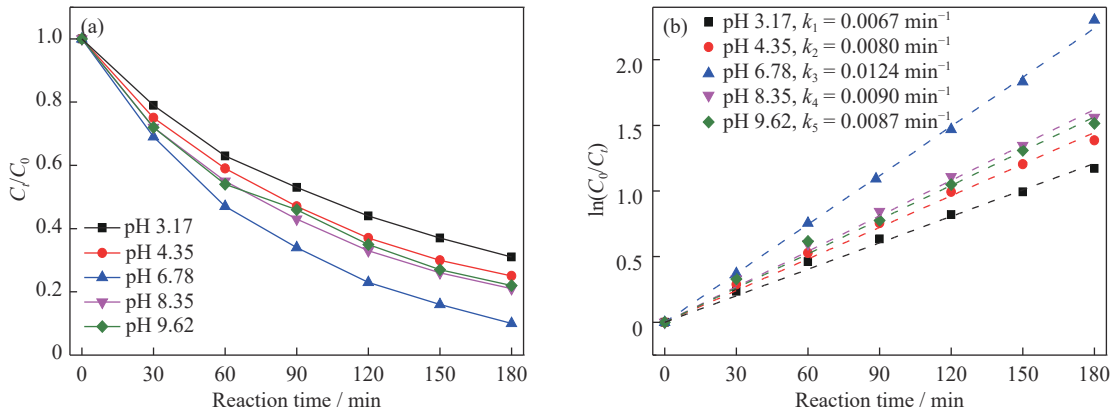

Fig. 13. Effect of the initial pH on (a) the decolorization efficiency of RhB and (b) the catalytic kinetics curves (25°C, catalyst concentration of 1.00 g·L^{-1}, and H_2O_2 dosage of 1.00vol%).

O_2 in alkaline solution, leading to less H_2O_2 adsorbed onto the ferrite, further affecting the reaction between the catalyst and H_2O_2 and decreasing the amount of •OH radicals [30]. Under this condition, the η of RhB decreased gradually from 90.0% to 78.0% and the k_{app} decreased from 0.0124 to 0.0087 min^{-1}. The results illustrate that a near-neutral but slightly acidic pH condition was beneficial for the removal of RhB; a pH value of 6.78 was therefore selected.

In conclusion, the optimum catalytic conditions were as follows: calcination temperature 1000°C, calcination time 2 h, pH 6.78, catalyst concentration of 1.00 $g·L^{-1}$, and H_2O_2 dosage of 1.00vol% with visible light irradiation. These conditions lead to a η value of 90% in 180 min.

3.4. Stability of as-prepared ferrite $Cu_{0.68}Zn_{0.32}Fe_2O_4$ over five cycles

Cycle experiments were necessary to study the stability of the as-synthesized catalyst under irradiation. The saturation magnetization (M_s) value of the obtained $Cu_{0.68}Zn_{0.32}Fe_2O_4$ was 54.62 $emu·g^{-1}$ (Fig. 14(a)), indicating the catalyst was a magnetic material that could be easily separated. The magnetic sample $Cu_{0.68}Zn_{0.32}Fe_2O_4$ was removed from the reaction solution by a strong magnet and then washed and dried. The results of experiments in which the same catalyst was used for five cycles (Fig. 14(b)) demonstrate that the decolorization efficiency of RhB decreased slightly after five cycles compared with that after the first cycle, still achieving 83.0%. The TOC removal efficiency (Fig. 14(c)) decreased from 45.0% to 36.7% after five cycles. In addition, XRD patterns of used and fresh ferrites (Fig. 14(d)) show no obvious change in the crystalline phase after five cycles, implying that the as-synthesized $Cu_{0.68}Zn_{0.32}Fe_2O_4$ was very stable and could be reutilized in the removal of RhB.

3.5. Environmental effect

To verify the toxicity of the EAFD and synthetic ferrite, the toxicity characteristic leaching procedure (TCLP) experiment was conducted. First, 1.0 g EAFD and 1.0 g ferrite were respectively mixed with HAc solution (pH = 2.88) under electromagnetic stirring at room temperature for 24 h. The solid–liquid separation was conducted by centrifugation, and the leachates were analyzed intensively using inductively coupled plasma optical emission spectrometry (ICP-OES, OPTIMA 7000DV, USA). The results are summarized in Table 4. According to the TCLP standard, the hazardous EAFD could be transformed to nontoxic Cu–Zn ferrite catalyst by the novel process proposed in this work.

In addition, the degraded RhB solutions were also measured; the results are shown in Table 5. The metallic ion concentrations in the RhB solutions after the first and fifth degradation were all below concentration limits specified in

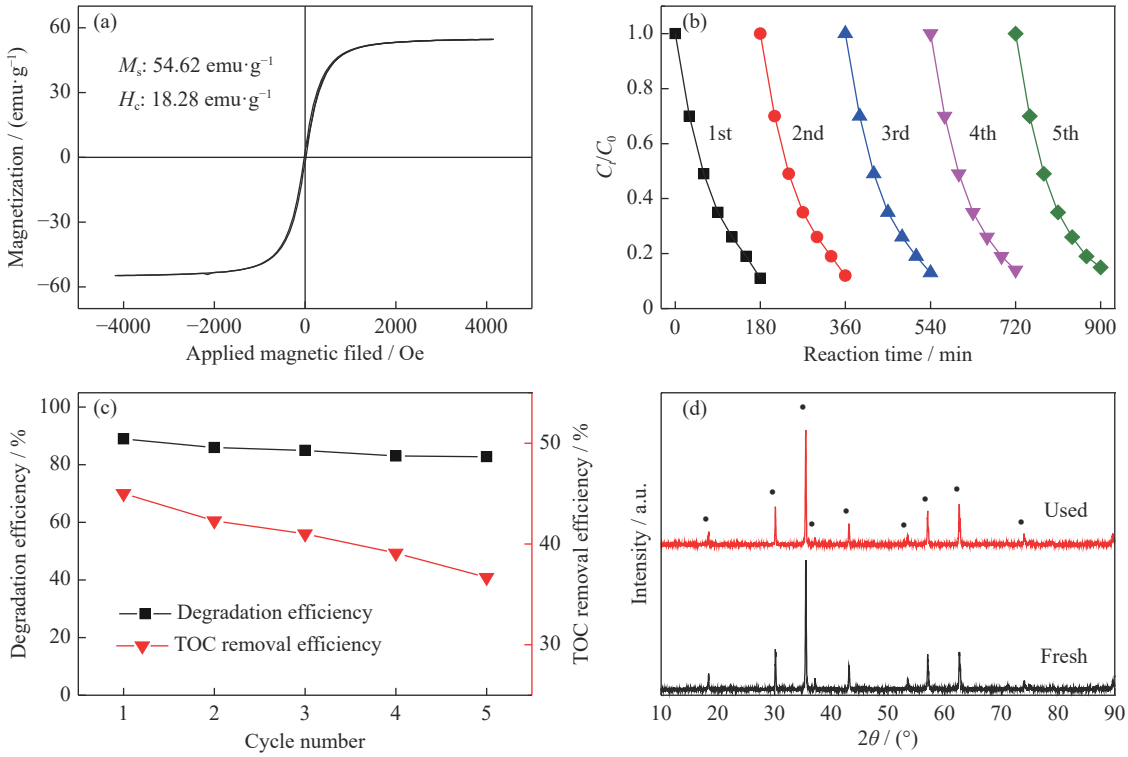

Fig. 14. (a) Room temperature hysteresis loops and the corresponding saturation magnetization (M_s) and coercive force (H_c) values; (b) results of a recycling study of the decolorization efficiency of RhB under optimal conditions; (c) decolorization efficiency and TOC removal efficiency of RhB in five cycle experiments; (d) XRD patterns of used and fresh samples synthesized at 1000°C for 2 h.

Table 4. Toxicity experiment results of Zn-containing EAFD and synthesized ferrite according to TCLP standard, as obtained by ICP-OES analysis mg·L^{-1}

Sample	Cr	Pb	Zn	Ni	Cd
Zn-containing EAFD	4.93	132.6	43.6	b.l.d	18.7
$(Cu_{0.68}Zn_{0.32})Fe_2O_4$	b.l.d	b.l.d	b.l.d	b.l.d	b.l.d
Maximum concentration	5	5	—	—	0.5

Note: b.l.d—below the limit of detection.

Table 5. Ion concentrations in RhB solutions by ICP-OES analysis and the emission standard (GB/31574—2015) mg·L^{-1}

Cycle number	Cu	Zn	Pb	As	Ni	Cr	Cd
1	b.l.d	b.l.d	0.103	b.l.d	b.l.d	b.l.d	b.l.d
5	b.l.d	b.l.d	0.097	b.l.d	b.l.d	b.l.d	b.l.d
Maximum concentration (GB/31574—2015)	0.2	1	0.2	0.1	0.1	0.5	0.01

emission standard GB/31574—2015, meaning that the degraded solutions could be discharged directly.

In our experiments, the $(Cu_{0.68}Zn_{0.32})Fe_2O_4$ ferrite obtained under the optimum preparation conditions of $R_{EAFD/Cu}$ = 2.0:0.9 and a calcination temperature of 1000°C and time of 2 h exhibited the best catalytic efficiency and the recovery ratio of the pretreated EAFD reached 90.7%, basically realizing the overall and high-value-added utilization of the toxic dust.

4. Conclusion

Nontoxic metal-doped $Cu_{0.68}Zn_{0.32}Fe_2O_4$ was successfully synthesized from hazardous Zn-containing EAFD through a solid-state reaction process, and it could be used as a Fenton catalyst. The effects of preparation parameters on the formation of ferrite catalyst and on the degradation of RhB were investigated in detail. The as-synthesized $Cu_{0.68}Zn_{0.32}Fe_2O_4$ exhibited the best decolorization efficiency of 90.0% in 180 min in the system of 0.2 g ferrite + 2 mL H_2O_2 + 200 mL 10 mg·L^{-1} RhB solution assisted by visible light irradiation. The cycling experiment demonstrated the good stability of the $Cu_{0.68}Zn_{0.32}Fe_2O_4$; the decolorization efficiency of RhB could still reach 83.0% after five cycles. In the meantime, the recovery ratio of the pretreated EAFD was 90.7%. The TCLP measurement illustrated the hazardous Zn-containing EAFD was turned into nontoxic ferrite and that the concentrations of metallic ions in the degraded RhB solutions were lower than the national emission standard, thereby demonstrating that the method proposed in this paper realized green and efficient use of the toxic EAFD.

Acknowledgements

This work was financially supported by the National Natural Science Foundation of China (No. U1810205), the National Basic Research Program of China (No. 2014CB 643401), and Shanxi Collaborative Innovation Center of High Value-added Utilization of Coal-related Wastes.

References

[1] V.N. Stathopoulos, A. Papandreou, D. Kanellopoulou, and C.J. Stournaras, Structural ceramics containing electric arc furnace dust, *J. Hazard. Mater.*, 262(2013), p. 91.

[2] P.E. Tsakiridis, A. Katsiapi, and S. Agatzini-Leonardou, Hydrometallurgical process for zinc recovery from electric arc furnace dust (EAFD). Part II: Downstream processing and zinc recovery by electrowinning, *J. Hazard. Mater.*, 179(2010), No. 1-3, p. 1.

[3] H.G. Wang, Y. Li, J.M. Gao, M. Zhang, and M. Guo, A novel hydrothermal method for zinc extraction and separation from zinc ferrite and electric arc furnace dust, *Int. J. Miner. Metall. Mater.*, 23(2016), No. 2, p. 146.

[4] F. Pinakidou, M. Katsikini, E.C. Paloura, P. Kavouras, T. Kehagias, P. Komninou, T. Karakostas, and A. Erko, On the distribution and bonding environment of Zn and Fe in glasses containing electric arc furnace dust: A μ-XAFS and μ-XRF study, *J. Hazard. Mater.*, 142(2007), No. 1-2, p. 297.

[5] H.W. Ma, K. Matsubae, K. Nakajima, M.S. Tsai, K.H. Shao, P.C. Chen, C.H. Lee, and T. Nagasaka, Substance flow analysis of zinc cycle and current status of electric arc furnace dust management for zinc recovery in Taiwan, *Resour. Conserv. Recycl.*, 56(2011), No. 1, p. 134.

[6] Y.C. Zhao and R. Stanforth, Integrated hydrometallurgical process for production of zinc from electric arc furnace dust in alkaline medium, *J. Hazard. Mater.*, 80(2000), No. 1-3, p. 223.

[7] C.C. Su and Y.H. Shen, Deflocculation and classification of electric arc furnace dust in aqueous solution, *Sep. Sci. Technol.*, 44(2009), No. 8, p. 1816.

[8] B. Liu, S.G. Zhang, B.M. Steenari, and C. Ekberg, Synthesis and properties of $SrFe_{12}O_{19}$ obtained by solid waste recycling of oily cold rolling mill sludge, *Int. J. Miner. Metall. Mater.*, 26(2019), No. 5, p. 642.

[9] H.G. Wang, M. Zhang, and M. Guo, Utilization of Zn-containing electric arc furnace dust for multi-metal doped ferrite with enhanced magnetic property: From hazardous solid waste to green product, *J. Hazard. Mater.*, 339(2017), p. 248.

[10] H.G. Wang, W.W. Liu, N.N. Jia, M. Zhang, and M. Guo, Facile synthesis of metal-doped Ni–Zn ferrite from treated Zn-containing electric arc furnace dust, *Ceram. Int.*, 43(2017), No. 2, p. 1980.

[11] J.M. Gao, M. Zhang, and M. Guo, Direct fabrication and characterization of metal doped magnesium ferrites from treated laterite ores by the solid state reaction method, *Ceram. Int.*,

41(2015), No. 6, p. 8155.
[12] E.G. Garrido-Ramírez, B.K.G. Theng, and M.L. Mora, Clays and oxide minerals as catalysts and nanocatalysts in Fenton-like reactions — A review, *Appl. Clay Sci.*, 47(2010), No. 3-4, p. 182.
[13] Y.B. Wang, H.Y. Zhao, M.F. Li, J. Fan, and G.H. Zhao, Magnetic ordered mesoporous copper ferrite as a heterogeneous Fenton catalyst for the degradation of imidacloprid, *Appl. Catal. B*, 147(2014), p. 534.
[14] J.H. Ramirez, F.J. Maldonadohodar, A.F. Pérez-Cadenas, C. Moreno-Castilla, C.A. Costa, and L.M. Madeira, Azo-dye Orange II degradation by heterogeneous Fenton-like reaction using carbon-Fe catalysts, *Appl. Catal. B*, 75(2007), No. 3-4, p. 312.
[15] Y.F. Diao, Z.K. Yan, M. Guo, and X.D. Wang, Magnetic multi-metal co-doped magnesium ferrite nanoparticles: an efficient visible light-assisted heterogeneous Fenton-like catalyst synthesized from saprolite laterite ore, *J. Hazard. Mater.*, 344(2018), p. 829.
[16] R. Sharma and S. Singhal, Spinel ferrite mediated photo-Fenton degradation of phenolic analogues: A detailed study employing two distinct inorganic oxidants, *Clean Soil Air Water*, 46(2018), No. 1, art. No. 1700605.
[17] G. Fan, T. Ji, and L. Feng, Visible-light-induced photocatalyst based on cobalt-doped zinc ferrite nanocrystals, *Ind. Eng. Chem. Res.*, 51(2012), No. 42, p. 13639.
[18] Y. Huang, C. Han, Y.Q. Liu, M.N. Nadagouda, L. Machala, K.E. O'Shea, V.K. Sharma, and D.D. Dionysiou, Degradation of atrazine by $Zn_xCu_{1-x}Fe_2O_4$ nanomaterial-catalyzed sulfite under UV–vis light irradiation: Green strategy to generate $SO_4^{\bullet-}$, *Appl. Catal. B*, 221(2018), p. 380.
[19] W. Zhao, C. Liang, B.B. Wang, and S.T. Xing, Enhanced photocatalytic and Fenton-like performance of CuO_x decorated $ZnFe_2O_4$, *ACS Appl. Mater. Interfaces*, 9(2017), No. 48, p. 41927.
[20] Z.K. Yan, J.M. Gao, Y. Li., M. Zhang, and M. Guo, Hydrothermal synthesis and structure evolution of metal-doped magnesium ferrite from saprolite laterite, *RSC Adv.*, 5(2015), No. 112, p. 92778.
[21] F. Tudorache, P. D. Popa, M. Dobromir, and F. Iacomi, Studies on the structure and gas sensing properties of nickel–cobalt ferrite thin films prepared by spin coating, *Mater. Sci. Eng. B*, 178(2013), No. 19, p. 1334.
[22] Y.L. Zhao, C.P. Lin, H.J. Bi, Y.G. Liu, and Q.S. Yan, Magnetically separable $CuFe_2O_4$/AgBr composite photocatalysts: Preparation. characterization. photocatalytic activity and photocatalytic mechanism under visible light, *Appl. Surf. Sci.*, 392(2017), p. 701.
[23] T. Mathew, N.R. Shiju, R. Sreekumar, S. Bollapragada, Gopinath, and S. Chinnakonda, Cu−Co synergism in $Cu_{1-x}Co_xFe_2O_4$-catalysis and XPS aspects, *J. Catal.*, 210(2002), No. 2, p. 405.
[24] C. Cai, Z.Y. Zhang, L. Jin, S. Ni, Z. Hui, and D.D. Dionysiou, Visible light-assisted heterogeneous Fenton with $ZnFe_2O_4$ for the degradation of Orange II in water, *Appl. Catal. B*, 182(2016), p. 456.
[25] H. Lin, Z. Hui, W. Xue, L. Wang, and W. Jie, Electro-Fenton removal of Orange II in a divided cell: Reaction mechanism, degradation pathway and toxicity evolution, *Sep. Purif. Technol.*, 122(2014), p. 533.
[26] Y.B. Wang, H.Y. Zhao, and G.H. Zhao, Iron-copper bimetallic nanoparticles embedded within ordered mesoporous carbon as effective and stable heterogeneous Fenton catalyst for the degradation of organic contaminants, *Appl. Catal. B*, 164(2015), p. 396.
[27] X. Zhong, J.B. Jr, D. Duprez, H. Zhang, and S. Royer, Modulating the copper oxide morphology and accessibility by using micro-/mesoporous SBA-15 structures as host support: Effect on the activity for the CWPO of phenol reaction, *Appl. Catal. B*, 121-122(2012), p. 123.
[28] X. Han, H.Y. Zhang, T. Chen, M. Zhang, and M. Guo, Facile synthesis of metal-doped magnesium ferrite from saprolite laterite as an effective heterogeneous Fenton-like catalyst, *J. Mol. Liq.*, 272(2018), p. 43.
[29] M. Dindarsafa, A. Khataee, B. Kaymak, B. Vahid, A. Karimi, and A. Rahmani, Heterogeneous sono-Fenton-like process using martite nanocatalyst prepared by high energy planetary ball milling for treatment of a textile dye, *Ultrason. Sonochem.*, 34(2017), p. 389.
[30] H. Hassan and B.H. Hameed, Fe–clay as effective heterogeneous Fenton catalyst for the decolorization of Reactive Blue 4, *Chem. Eng. J.*, 171(2011), No. 3, p. 912.